Hydrological Processes

WILEY

RESEARCH ARTICLE OPEN ACCESS

Wood-Biochar Influence on Rill Erosion Processes and Hydrological Connectivity in Amended Soils

Pellegrino Conte[1] | Calogero Librici[1] | Alessio Nicosia[1] | Vincenzo Palmeri[1,2] | Vincenzo Pampalone[1] | Vito Ferro[1,2]

[1]Department of Agricultural, Food and Forest Sciences, University of Palermo, Palermo, Italy | [2]NBFC, National Biodiversity Future Center, Palermo, Italy

Correspondence: Alessio Nicosia (alessio.nicosia@unipa.it)

Received: 4 November 2024 | **Revised:** 16 December 2024 | **Accepted:** 9 February 2025

Funding: The authors received no specific funding for this work.

Keywords: hydrological connectivity | nuclear magnetic resonance | pore distribution | pore size | relaxometry | rill erosion | soil loss | wood-biochar amended soil

ABSTRACT

Although there is increasing interest in biochar as a soil amendment, its antierosive effectiveness is still uncertain. This investigation aims at evaluating how wood-biochar affects rill erosion and hydrological connectivity in amended soils. In this paper, at first, plot experiments were performed entering a clear inflow into two rills, named $rill_3$ and $rill_5$, incised in a soil amended with an initial biochar concentration *BC* in weight of 3% and 5%, respectively. For each rill, terrestrial photogrammetry was used to obtain the Digital Elevation Models (DEM) before and after the experimental runs, and the consequent DEM of difference (DoD) was used to calculate the total volume of the eroded mixture (sediment and biochar), while three samples of rill outflow discharge were collected to determine the biochar and sediment rates. Then, small laboratory samples of the soil, biochar, and mixtures with different *BC* (1%, 3%, 5%, 10%, and 30%) were used to determine size and distribution of pores, and thus measure the structural and functional connectivity, by nuclear magnetic resonance (NMR) relaxometry with the fast field cycling (FFC) layout. The DoDs highlighted that the mixture volume for $rill_5$ was lower than that for $rill_3$. Moreover, the $rill_5$ condition yielded a higher biochar percentage in the mixture. The NMR measurements demonstrated that the biochar addition increases the size of micropores and mesopores, and the macro-pore component is never dominant. Biochar concentrations greater than 5% do not produce appreciable changes in the pore distribution inside the mixture. The biochar component improves the structural connectivity up to $BC = 5\%$. In the *BC* range of 0%–3%, *FCI* decreased as *BC* increased. In conclusion, a target biochar concentration of 5% allows for the mitigation of the rill erosion phenomena, favours the improvement of soil structural connectivity, and does not appreciably modify the functional connectivity.

1 | Introduction

Soil erosion is one of the main environmental threats (Borrelli et al. 2017), whose effects are often underestimated and whose relevance is confirmed by several field investigations (Bagarello et al. 2008, 2011, 2018). Soil formation is an extremely slow process, while its use causes accelerated soil loss. Soil loss in agricultural land is 10–40 times greater than the rate of soil formation; slope protection is often inadequate, and interventions to prevent hydrogeological risk are rare (Carollo et al. 2023). Soil water erosion has both on-site (e.g., reduction of soil fertility and productivity) and off-site (e.g., deposition of sediments in rivers and artificial reservoirs) impacts (Di Stefano and Ferro 2016; Di Stefano et al. 2023). It also contributes to global warming due to the release of CO_2 into the atmosphere, caused by the oxidation of enormous quantities of organic carbon (Pimentel 2006). Finally, careless and opportunistic use of land has reduced its ecosystem services (Carollo et al. 2023).

Rill erosion is due to soil particle detachment and transport by channelized flows. In comparison with overland flows, rills are featured by higher flow shear stresses and velocities, which determine higher values of sediment yield. Rills are eroded channels that rapidly change their own morphology (Di Stefano et al. 2022a), representing a significant sediment source and determining most of the sediment transport on hillslopes (Mutchler and Young 1975; Zhang et al. 2016). The transport of soil particles detached by rill flow and those delivered from the interrill areas to rills is usually facilitated by the formation of a rill network (Bagarello and Ferro 2010; Bagarello et al. 2015; Di Stefano et al. 2013, 2015; Bruno et al. 2008; Govers et al. 2007; Peng et al. 2015). Rill erosion is a severe problem worldwide and regards many areas characterised by different climates, soil uses, soil, topography, etc. The large interest in this erosion phenomenon is testified by the geographical spread of studies available in the literature in Africa (Heri-Kazi and Bielders 2021), Asia (Huang et al. 2015; Parhizkar et al. 2021), Europe (Wirtz et al. 2012; Di Stefano et al. 2019, 2022b), America (Polyakov and Nearing 2003), and Australia (Lu et al. 2003).

In a context in which farmers tend to avoid the use of cover crops to control soil erosion as they compete with the main crop for water and nutrients (Guerra and Steenwerth 2012; Novara et al. 2021), alternative soil conservation practices aimed at the limitation of soil erodibility appear to be a valid solutions to mitigate erosion processes. However, chemical additives able to improve soil structure may be subject to leaching and are only effective for heavy, fine-textured soils (Waddington 1992). Furthermore, the use of most synthetic additives is prohibited or severely limited in organic farming. For these reasons, organic amendments, such as biochar or compost, can be considered a valid and eco-friendly alternatives for soil amendment (Schmidt et al. 2014).

Biochar is obtained from the pyrolysis of biomass in the partial or complete absence of oxygen (Sohi et al. 2010). Generally, it positively influences the overall quality of a soil (Blanco-Canqui 2017), improves its structure (size, arrangement, and aggregate stability), increases its organic matter, and determines the increase in crop production and quality (Wang and Wang 2019). As biochar is characterised by a very low degradation rate, the positive effects on the chemical, physical, and biological soil characteristics can persist for long periods of time (Atkinson et al. 2010; Castellini et al. 2015). Biochar significantly affects the mechanical and hydraulic soil properties, and its erosion control action has been evaluated in some experimental investigations.

Jien and Wang (2013) tested the influences of different biochar concentrations *BC* (0%, 2.5%, and 5% in weight (100 × g biochar/g total soil)) applied to a long-term cultivated acidic Ultisol (43.6% clay, 40.2% silt, and 16.2% sand). For each treatment, soil loss due to a single simulated rainfall event with an intensity of $80\,mm\,h^{-1}$ was measured. An appreciable reduction of soil loss (50% and 64% at 2.5% and 5% application rates, respectively) was detected in comparison with the condition of non-amended soil. These authors concluded that the incorporation of biochar improves the soil's physical properties, and the formation of macroaggregates is the factor controlling soil erosion.

Li et al. (2019) studied the influence of biochar on soil erosion phenomena using different *BC* values (1%, 3%, 5%, and 7% in weight) and three different biochar particle sizes (2–1, 1–0.25, and < 0.25 mm). The rainfall simulation ($90\,mm\,h^{-1}$) experiments were carried out on a small plot (1 m long, 0.8 m wide, 0.4 m deep), filled with silt loam soil (8.93% clay, 60.87% silt, and 30.2% sand), using a slope of 27%. The experiments demonstrated that generally lower (1% and 3%) *BC* inhibits soil loss, and higher (5% and 7%) *BC* promotes it. The best treatment for reducing runoff and soil loss was obtained by combining a *BC* of 1% with biochar particles smaller than 0.25 mm.

Li et al. (2020), using the same silt loam soil and experimental layout as Li et al. (2019), established that biochar with coarse particle size (1–2 mm) is better retained in soils, and biochar concentrations less than or equal to 3% allow for reducing soil degradation due to erosion processes.

Sadeghi et al. (2016) carried out some experimental runs using a small plot ($0.25\,m^2$) with sandy clay loam soil, having a slope of 20%, amended by vinasse-produced biochar. The runs were conducted using a biochar application rate of $8\,t\,ha^{-1}$ distributed on the soil surface 24 or 48 h before the rainfall simulation ($50\,mm\,h^{-1}$). These experiments demonstrated that the application of biochar reduces runoff volume, soil loss, and sediment concentration rates.

Zhang et al. (2019) highlighted that contrasting results on significant mitigation of soil erosion by biochar addition were reported in the literature. In fact, some authors (Lee et al. 2018; Li et al. 2017, 2019) concluded that biochar addition can promote soil erosion, while other research (Abrol et al. 2016; Doan et al. 2015; Hseu et al. 2014; Jien and Wang 2013; Lee et al. 2015; Sadeghi et al. 2016; Smetanová et al. 2013) support the hypothesis that it reduces soil susceptibility to erosion.

These inconsistent results can be justified considering the differences due to the biochar type and particle size, the investigated soil, the method applied for adding biochar (spread over the soil surface, incorporated into the soil), the vegetation growth, and the change in physical and chemical soil properties due to biochar addition (Wani et al. 2021). In particular, the method applied to add biochar has a direct effect on runoff and soil loss. When the biochar is spread on the soil surface (Sadeghi et al. 2016; Smetanová et al. 2013), a biochar surficial layer is formed and protects the soil structure, inhibits seal formation, favours infiltration processes, and limits soil particle detachment, thus reducing runoff and soil loss. The spreading of biochar on the soil surface is also impractical as low-density biochar particles are characterised by high transportability (Sadeghi et al. 2016). As a consequence, this type of biochar addition increases the erosion of low-density biochar particles and reduces soil loss. In field applications, biochar is usually added inside the arable soil horizon and thoroughly mixed to favour the improvement of soil properties.

Zhang et al. (2019) suggested that biochar addition alters soil erodibility, and the variation of this soil property could exhaustively justify the role of biochar addition against erosive phenomena. The experiments by Zhang et al. (2019) were carried out using small, perforated metal boxes (0.45 m long, 0.3 m wide, and 0.10 m deep), having a slope gradient of 17%, subjected to simulated rainfalls with four intensities (25, 50, 75, and 100 mm h^{-1}). They used three biochar concentrations (2%, 5%, and 8% by weight) and two incubation periods (no incubation and a 140-day incubation). The addition of biochar to the investigated clay loam soil reduced the soil bulk density, delayed the seal formation, and reduced the soil compactness (Busscher et al. 2010; Doan et al. 2015; Herath et al. 2013) determining an adverse effect on soil erodibility. The interrill erodibility of the biochar-added soil increased 20%–30% as compared to that of the original soil.

Recently, Gholamahmadi et al. (2023) developed a meta-analysis of biochar impacts on runoff and soil erosion and concluded that the best soil erosion mitigation strategy is obtained by incorporating biochar into the topsoil to 15 cm or less and using biochar concentrations between 0.6% and 2.5%. *BC* values greater than 2.5% provoked no significant reduction in soil erosion.

For two cultivated soils (silt loam and sandy loam), Zanutel and Bielders (2023) investigated the effects of short-term (fresh) and long-term (century-old) biochar and concentration *BC* (1% and 2%) on interrill erosion. The addition of biochar to the silt loam soil was ineffective, while the increase of *BC* from 1% to 2% determined a reduction of interrill erosion for the sandy loam soil.

Currently, most of the available studies concern interrill erosion under simulated rainfall, while few investigations on rill erosion are available (Li et al. 2021; Nicosia et al. 2021; Parhizkar et al. 2023; Li et al. 2025). Li et al. (2021) conducted some experiments ($BC = 1.4\%$ and 3%) on the susceptibility to rill formation, observing a decreased susceptibility with the biochar addition. Nicosia et al. (2021), using the data collected by Li et al. (2021), demonstrated that the biochar addition reduced the flow Froude number due to the increase in roughness, which determined the decrease in flow velocity and the increase in water depth. Parhizkar et al. (2023) studied the effect of rice husk-biochar on rill erosion by carrying out experiments in a flume (3.5 m long and 0.2 m wide) with both non-amended soil and soil amended with 3% biochar by weight. They found that biochar reduced rill erodibility and critical shear stress for the investigated silty-clay soil. Furthermore, Parhizkar et al. (2023) found greater aggregate stability and a lower bulk density of the treated soil compared to the non-amended one. Recently, Li et al. (2025) investigated the impact of biochar on rill erodibility K_r and critical shear stress τ_c in order to assess a relationship between K_r, τ_c and soil properties. In comparison with no biochar addition, they established that the addition of 1%–4% biochar after 1–2 years generally determined a reduction of K_r and an increase of τ_c. In other words, the addition of 1%–4% biochar concentration can be considered an effective soil conservation practice that enhances soil resistance to rill erosion (Di Stefano et al. 2016).

However, the available literature regarding biochar effects on rill erosion is still lacking and needs to be widened by testing the influence of different types of biochar under different experimental conditions (e.g., soil texture, slope, discharge, etc.).

The impact of biochar use as a soil conservation practice can be assessed not only by quantifying soil loss values obtained for different experimental conditions, but also by determining the interactions between amended soil particles and water, which drive several phenomena such as water infiltration and the formation of surface runoff. In this sense, studies about the biochar effect on hydrological connectivity in amended soils, determining pore size and distribution, can be a valid tool to better understand how biochar affects soil structure and its interplay with soil erosivity.

The word "connectivity" states the way in which an environmental system favours matter and energy movement inside or among its elements (Pringle 2003; Bracken and Croke 2007; Marchamalo et al. 2016; Keesstra et al. 2020). This concept aims to stand for the attitude of a vector, such as water, to transport materials at different spatial and temporal scales (Bracken et al. 2013; Reaney et al. 2014; López-Vicente et al. 2017), accounting for both the heterogeneity and complexity of a heterogeneous environmental system.

According to Wainwright et al. (2011), an environmental system can be characterised by *structural* (*SC*) and *functional* (*FC*) connectivity. The former (*SC*) states the physical proximity of different characteristics and their reciprocal link (Belisle 2005; Turnbull et al. 2008; Baartman et al. 2013). Therefore, structural connectivity expresses how the investigated process is affected by the interactions among the structural characteristics of a given system (Uezu et al. 2005). The second one (*FC*) establishes how a specific process (e.g., hydrological) is affected by the interactions among the structural components and the considered vector (Wainwright et al. 2011). For the soil system, soil texture and particle arrangement can be used to define soil structural connectivity, and the physico-chemical interaction between the system and water defines the functional component. These two components influence water infiltration within the soil. According to these definitions, structural connectivity provides a time-independent (stationary) response of the examined system, while functional connectivity reflects a dynamic viewpoint.

Conte and Ferro (2018, 2020, 2022) presented the idea of "hydrological connectivity inside the soil" (HCS) to express how the water movement inside the soil is influenced by the interaction of soil spatial patterns (i.e., *SC*) with chemical and physical processes (i.e., *FC*). In this context, the *SC* considers the spatial arrangement of channels and soil pores, while the *FC*, expressing the water transfer inside soil pores, is related to the influence given by the water, which physico-chemically interacts with the pore edges (Conte et al. 2017).

To the best of our knowledge, the literature lacks studies focused on *HCS* for biochar-amended soils. Moreover, as mentioned above, only a few studies have investigated rill erosion in biochar-amended soils. Consequently, the biochar's effectiveness against rill erosion can be further investigated by performing experiments to measure the differences in terms of soil loss

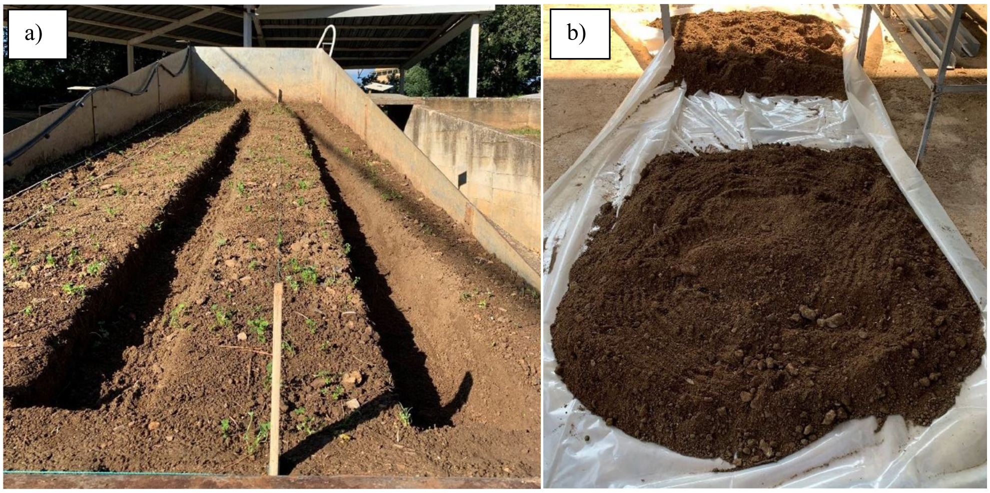

FIGURE 1 | View of the experimental plot with the two trenches (a) and soil piles (b).

and hydrological connectivity determined by the addition of different types of biochar and biochar concentrations.

The general aim of this study is to investigate the wood-biochar influence on rill eroded volumes and hydrological connectivity in amended soils. In detail, in this study, experimental measurements performed on rills formed in soils amended with two different concentrations of wood-biochar (3% and 5%) are used with the specific aims to: (i) compare the eroded volumes determined by the same inflow; and (ii) analyse the mixtures of eroded sediment and biochar outflowing from the rills to determine the content of sediment and biochar in the eroded volume for each rill. Then, nuclear magnetic resonance (NMR) relaxometry with the fast field cycling (FFC) layout is used to measure the structural and functional connectivity of the original soil, the biochar, and the mixtures with different biochar concentrations (1%, 3%, 5%, 10%, and 30%) with the aim to test if the increase of *BC* produces appreciable changes in the pore distribution inside the mixture and if the connectivity properties are related to soil erosion phenomena.

2 | Materials and Methods

2.1 | Measurements of Rill Erosion and Evaluation of the Sediment and Biochar Components

The experimental measurements were performed on a plot 2 m wide and 7 m long (Figure 1a), located at the Department of Agricultural, Food, and Forestry Sciences (University of Palermo, Sicily, Italy). The plot is filled with clay-loam soil (32.7% clay, 30.9% silt, and 36.4% sand) with an average slope of 15%. Two trenches (Figure 1a), 5.7 m long, 0.2 m wide, and 0.1 m deep, were dug for a total removal of approximately 100 kg of soil per trench. The soil was distributed on plastic sheets in piles and left to air-dry for a week (Figure 1b). Then, three samples were taken and weighed from each pile, and subsequently oven-dried at 105° for 24 h to determine the gravimetric soil moisture, which was equal to 12.5%. The pre-established wood-biochar (bulk density = 0.26 g cm^{-3}, porosity = 0.65 cm^3 cm^{-3}) concentration *BC* of 3% (rill$_3$) and 5% (rill$_5$) was reached by adding 300

FIGURE 2 | View of the preferential path (a) and flow moving into the rill (b).

and 500 g of biochar to 10 kg of soil in dry weight, corresponding to approximately 11.4 kg in wet weight, due to the given soil moisture. The mixing phase between soil and biochar was performed for 60 s by a concrete mixer, and then the amended soil was put back into the trenches and compacted. A preferential path (Figure 2a), slightly incised and having two converging sides, was established on the surface of the 0.2 m wide amended area, and after 2 weeks (i.e., the time within which biochar modifies soil characteristics (Joseph et al. 2010)) the experimental runs were performed. At the beginning of the experimental run, the preferential path was modelled by the clear flow discharge (0.22 L s^{-1}) to shape an actual rill (Figure 2b) characterised by a maximum measured width of 0.09 m. For each rill, during the run, a sample of rill outflow discharge was collected by a steel pan (0.555 m long and 0.265 m wide) at three different sampling times (t_0 = 2 min, t_1 = 8 min, and t_2 = 11 min after the beginning of the experimental run) (Figure 3) for 30 s. The volume of the six (2 rills × 3 sampling times) collected samples (water + sediments + biochar) varied in the range 2.5–3.8 L. The samples were oven-dried at 105°C for 48 h and then weighed to determine the amount of eroded mixture (sediments and biochar). From these samples, sub-samples of 10 g were collected by a rotating laboratory mixer, which assures the homogeneity of the sub-samples.

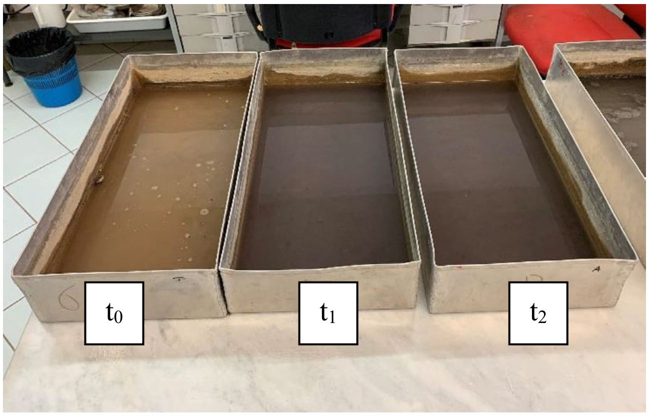

FIGURE 3 | Samples collected from the outflow of each rill at different sampling times.

As the biochar is made of organic matter, these sub-samples were put in a muffle furnace at 400°C to determine the loss on ignition *LOI* (%), that is, the total organic matter burned at this temperature. Two undisturbed soil samples were also collected and put into the muffle furnace to determine the organic matter *OM* (%), which was equal to 2%. This baseline value was subtracted from the *LOI* to determine the biochar percentage *BC* in the mixtures.

The weight of biochar in the eroded mixtures (sediment and biochar) was determined by multiplying the sample dry weight by the biochar percentage in the mixture. The biochar weight was converted into volume by using the biochar bulk density of 0.26 g cm^{-3}, and the volumetric biochar discharge was then calculated by the ratio of the volume to the sampling time (30 s).

For rill$_3$ and rill$_5$, the three values of biochar discharges were averaged, and these mean values were multiplied by the run duration (12 min) to obtain the total biochar volumes V_{BIO3} and V_{BIO5}.

The three-dimensional Digital Terrain Model (3D-DTM) was created by a 3D-photo reconstruction technique using a set of approximately 70 photographs taken from the plot area by a digital camera. From the 3D-DTM, the Digital Elevation Models (DEM) before (D1) and after the experimental runs (D2) were obtained. The total eroded mixture volumes, V_3 for rill$_3$ and V_5 for rill$_5$, were calculated by the DEM of difference (DoD) (Figure 4) between D2 and D1. The sediment volumes in the mixture, V_{s3} and V_{s5}, were determined as the difference between V_i and V_{BIOi}, with $i = 3$ and 5.

2.2 | Assessing Hydrological Connectivity Inside a Soil (HSC)

NMR relaxometry joins different NMR techniques to observe how quickly the z-component of the nuclear magnetic moment (i.e., the bulk nuclear spin magnetization) changes from a non-equilibrium state to the equilibrium distribution. Fluctuations of local magnetic or electrical fields generate a phenomenon named relaxation, which is mainly due to molecular motions. Therefore, measurements of the relaxation times (both longitudinal, T_1, and transversal, T_2) are expressive of the molecular dynamics.

FIGURE 4 | DEM of difference (DoD) obtained for the rills with a biochar concentration of 3% (rill$_3$) and 5% (rill$_5$).

The T_1 values provide information about motion frequencies ranging from 105 to 108 Hz (Laudicina et al. 2012; De Pasquale et al. 2012), which are the typical ones for water molecule movement in porous media. If the porous medium is soil, the shortest T_1 are associated with small-sized pores (i.e., pores bounded by clay primary particles and small aggregates), while the longest T_1 correspond to pores bounded by sand particles, silt, and large aggregates (Pohlmeier et al. 2009; Conte et al. 2017).

Conte and Ferro (2018, 2020, 2022) presented a method for defining the SC and FC of a soil by introducing a new mathematical use of the relaxograms obtained by NMR relaxometry. The quantification of SC and FC was made by using the structural connectivity index *SCI* and functional connectivity index *FCI*, calculated considering the NMR relaxogram shapes. In detail, for a given proton Larmor frequency, the relaxogram (Figure 5a) is integrated, and T_1, the area, A_{T1}, under the relaxogram (Figure 5a) is calculated. Figure 5b plots an example of the integral curve of the relaxogram, that is, the T_1-A_{T1}/A curve, where A is the entire area under the relaxogram. The ratio A_{T1}/A ranges from 0 to 1 and is equal to the non-exceeding empirical cumulative frequency, $F(T_1)$, of the longitudinal relaxation time. Conte and Ferro (2018, 2020, 2022) demonstrated that $F(T_1)$ is S-shaped and found two points (A and B in Figure 5b) characterised by a sudden change in the curve slope. The A point bounds a part of the curve characterised by the shortest T_1 falling within the range T_A (Figure 5b), while the B point limits the part characterised by the longest T_1 falling in the T_B range (Figure 5b). Conte and Ferro (2018, 2020, 2022) set the A and B points with the aim of identifying the two extreme components of the S-shaped $F(T_1)$ distribution: point A, with an ordinate of $F(T_1)=0.01$, and point B, with an ordinate $F(T_1)=0.99$. The value $F(T_1)=0.01$ distinguishes the low component (only 1% of the measured T_1 values are less than the abscissa characterising the point A), whereas $F(T_1)=0.99$ distinguishes the high component (only 1% of the measured T_1 values are higher than the abscissa characterising this point).

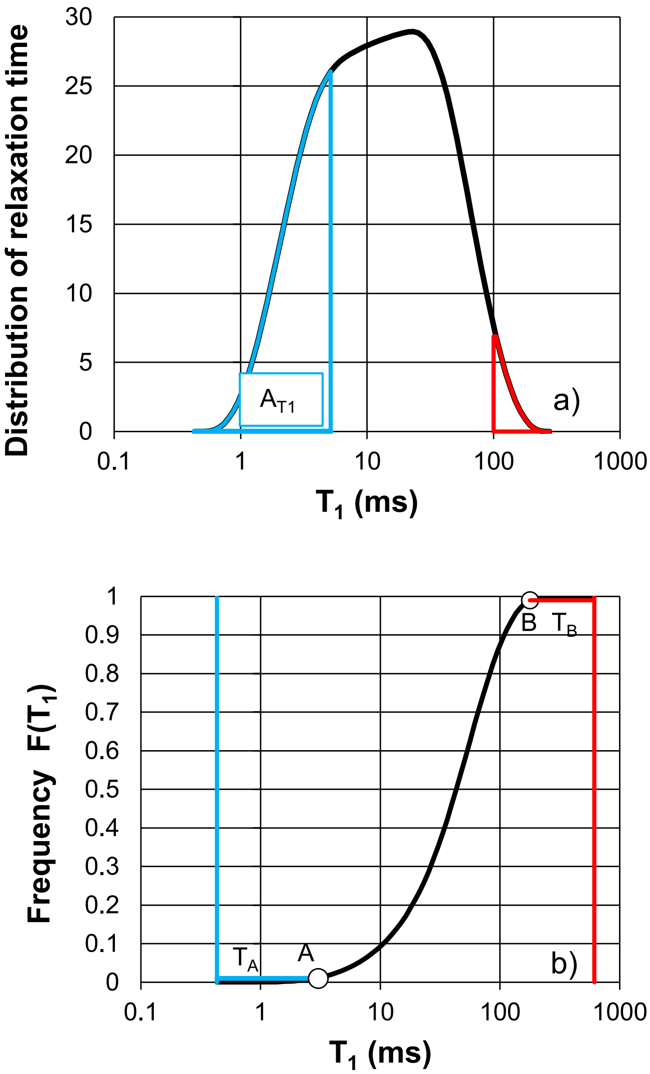

FIGURE 5 | Examples of relaxogram (a) and the derived integral curve (b).

The water movement in macro- (> 50 μm), meso- (0.5–50 μm), and micro- (< 0.5 μm) pores is considered in terms of the hydrological connectivity inside the soil (Pagliai and Vignozzi 2002). Associating the relaxation times with pore sizes, the low component of the $F(T_1)$ distribution identifies micro-pores, where limited space causes a reduction in water molecular movement. The high component is related to macro-pores, which are characterised by wide water mobility. Water molecules moving within the micro-pores have a range of T_1 values near the lower T_1 limit (T_A in Figure 5b), while molecules moving within the macro-pores are characterised by T_1 values near the upper T_1 limit (T_B in Figure 5b) of the measured relaxation time distribution. Water molecules moving within meso-pores are identified by all the T_1 values falling between A and B points. In other words, bulk water movement is related to the limb of the $F(T_1)$ curve (bounded by the A and B points of Figure 5b), whereas the high and low components of $F(T_1)$ refer to water interacting with the soil pore edges. Further details regarding the interactions between the pore surfaces and water molecules are reported in previous papers (Pohlmeier et al. 2009; Conte et al. 2017; Conte 2019).

Conte and Ferro (2018, 2020, 2022) proposed the ratio T_B/T_A as *FCI*. This definition allows for considering that the T_1 values in the range T_A identify water inside small pores, whereas those in the range T_B correspond to water within large pores. According to the definition of *FCI*, both increasing T_A and/or decreasing T_B decreases the index values.

Conte and Ferro (2018, 2020, 2022) proposed using the AB limb zone of the $F(T_1)$ curve (Figure 5b) to calculate the *SCI*. Considering the relationship between T_1 and pore size, the *SCI* was defined as the coefficient of variation of T_1 values characterised by $0.01 < F(T_1) < 0.99$.

2.3 | FFC NMR Instrument, Investigated Samples and Data Analysis

A Stelar SmarTracer Fast-Field-Cycling NMR Relaxometer (Stelar s.r.l., Mede, PV–Italy) at a constant temperature of 25°C was used to carry out the relaxometry experiments. The instrument works by rapidly switching among three different magnetic fields, which are set to account for NMR sensitivity (polarisation field, B_{POL}), relaxation (relaxation field, B_{RLX}), and acquisition (acquisition field, B_{ACQ}). The latter is used to maintain the observable magnetisation (generated for the present study by applying a 4.71 μs 90° pulse right after BRLX application) for a period of time named acquisition time. The relaxation field is varied in the proton Larmor frequency ν_L comprised in the interval 0.01–10 MHz, which is the working range of the used equipment. B_{POL} is used only when B_{RLX} is in the range 0.01–3 MHz. In particular, the polarisation field—corresponding to a proton Larmor frequency of 10 MHz—is applied for a period (T_{POL}) of about five times the T_1 estimated at the selected frequency. Switching dead time was 3 ms, while a recycle delay of 4 s has been used.

Finally, the Uniform PENalty regularisation (UPEN) algorithm (Borgia et al. 1998; Conte 2019) was used to achieve the distribution of the longitudinal relaxation times to assess the hydrological connectivity inside a soil (HCS).

For each soil, following the result of Conte and Ferro (2020), the distribution of T_1 was obtained using a sample-to-water ratio in weight of 1:0.25, corresponding to the water holding capacity WHC, at a proton Larmor frequency ν_L varying from 0.01 to 10 MHz. In other words, the experimental runs were carried out with a single value of WHC and different values of ν_L. Each laboratory sample was prepared in a beaker, and then the slurry sample was manually transferred into the NMR tubes to obtain homogeneous packing. The FFC NMR measurements were carried out for the soil and the biochar used for the rill runs, and the mixtures prepared in the laboratory with different biochar concentrations (1%, 3%, 5%, 10%, and 30%). Three repetitions of NMR measurements were carried out for each investigated sample.

3 | Results

3.1 | Rill Erosion in Biochar-Amended Soils

The obtained DoD (Figure 4) highlights that the mixture volume ($V_5 = 6.3$ L) for the rill$_5$ is lower than that ($V_3 = 7.0$ L) for the rill$_3$ and, therefore, the higher initial biochar concentration reduced the rill erosion phenomenon.

The biochar volumes in rill$_3$ (V_{BIO3}) and rill$_5$ (V_{BIO5}) were equal to 1.59 L and 2.08 L, respectively. These values were divided by the total eroded volumes obtained by the DoD, resulting in a biochar percentage in the mixture of 22.7% (rill$_3$) and 32.8% (rill$_5$). Finally, the treatment with the higher biochar initial concentration ($BC = 5\%$) decreased the overall erosive phenomenon ($V_3 = 7.0$ L and $V_5 = 6.3$ L) and produced a higher biochar percentage in the mixture. The sediment volumes of the two rills, V_{s3} and V_{s5}, were then equal to 5.4 and 4.2 L and, therefore, pointed out a 1.2 L reduction in sediment volume between rill$_5$ and rill$_3$.

3.2 | Hydrological Connectivity of Biochar-Amended Soils

At first, to calculate the *FCI* and *SCI* indexes, the cumulative frequency distributions of the longitudinal relaxation time for the relaxograms corresponding to the original soil (S), the applied biochar (BIO), and the mixtures (M, x) of soil with different percentages of biochar ($x = 1\%$, 3%, 5%, 10%, and 30%) acquired at the different applied magnetic fields were examined. Figure 6 shows as an example for four values of the applied magnetic field having a known proton Larmor frequency ($\nu_L = 0.01$, 0.8, 5, and 10 MHz), the detected longitudinal relaxation time distribution. For each ν_L value, the $F(T_1)$ distribution of the soil is always to the left of the $F(T_1)$ corresponding

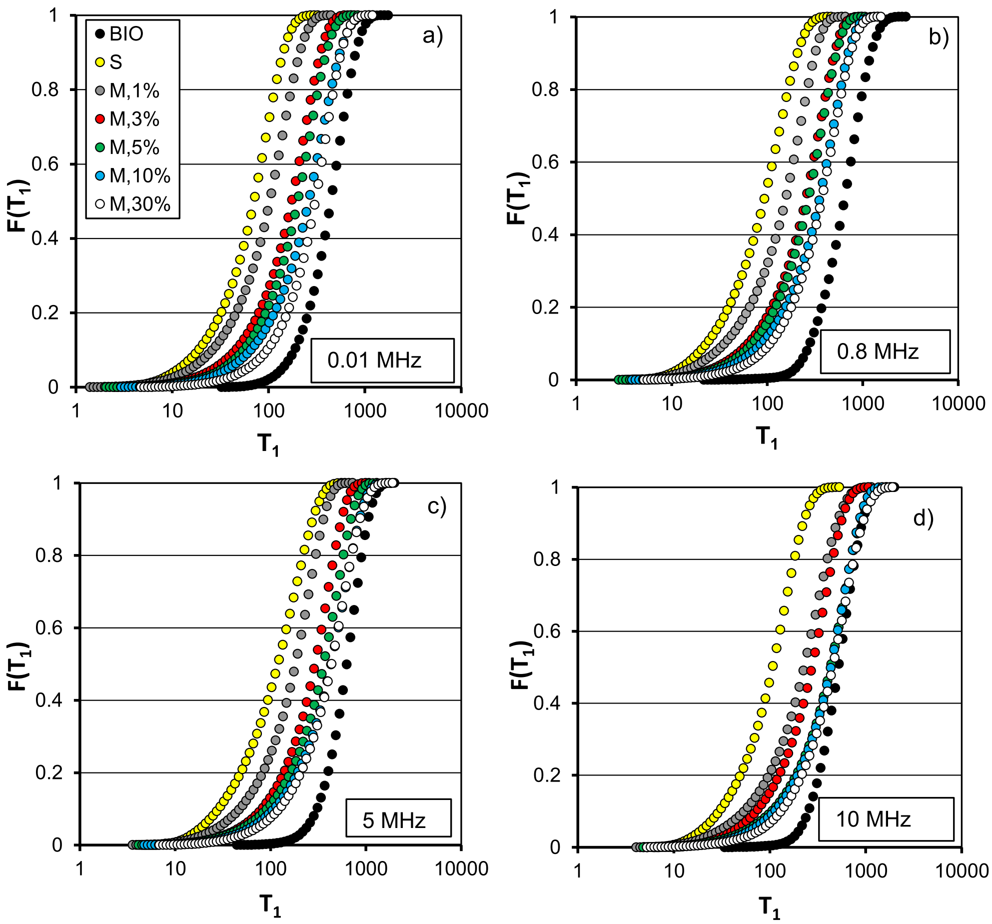

FIGURE 6 | Cumulative frequency distributions $F(T_1)$ of the investigated samples (biochar BIO, soil S, and mixture M, x, in which x is the biochar concentration), for different applied proton Larmor frequencies in the range 0.01–10 MHz.

to the investigated mixtures and biochar, while the $F(T_1)$ for the biochar is always to the right of the distributions related to the mixtures.

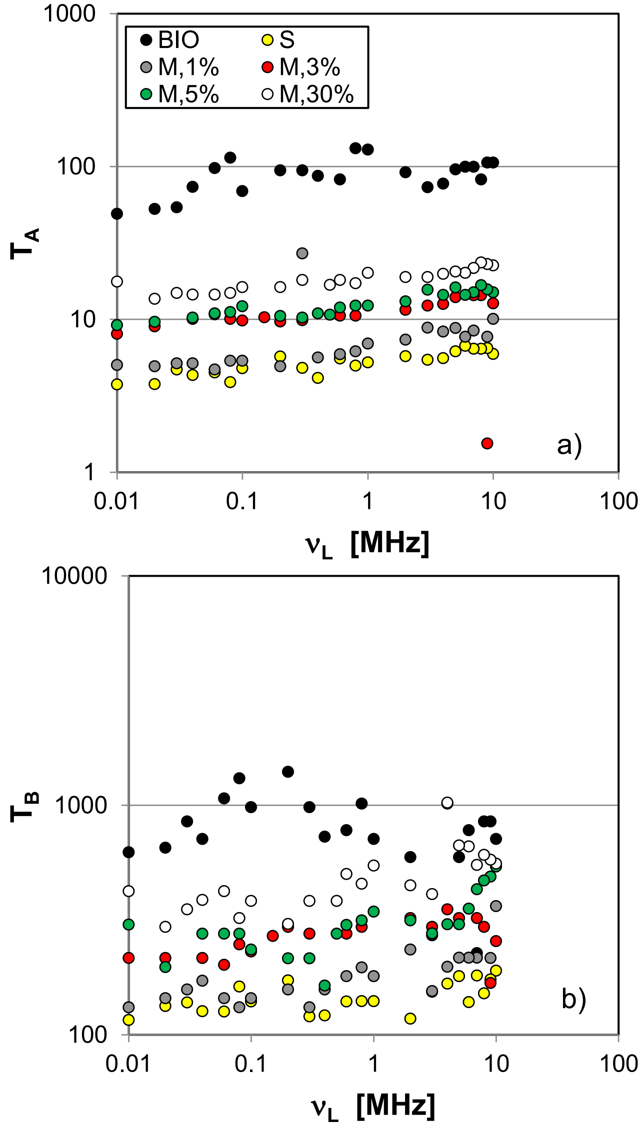

FIGURE 7 | Relationship between the applied proton Larmor frequency ν_L and T_A (a) and T_B (b) for all the investigated samples (biochar BIO, soil S, and mixture M, *x*, in which *x* is the biochar concentration).

For all samples, Figure 7 shows the variations of T_A, corresponding to water molecules inside small pores, and T_B, corresponding to water within large pores, with ν_L and demonstrates that the highest T_A and T_B values correspond to the biochar; the lowest values feature the soil, and T_A and T_B increase with the biochar percentage. Figure 7 also highlights that the T_A and T_B values are independent of ν_L, and the corresponding mean values, $m(T_A)$ and $m(T_B)$, are listed in Table 1. The values listed in Table 1 show that $m(T_A)$ and $m(T_B)$ increase with the biochar component.

Figure 8 shows how the structural connectivity index *SCI* (Figure 8a) and the functional one *FCI* (Figure 8b) vary with the applied magnetic field and the percentage of biochar. The existence of an advisable upper limit for the biochar percentage is also disclosed for *SCI* and *FCI*.

According to a previous study (Conte and Ferro 2020), the *SCI* and *FCI* values of the mixtures measured by applying different magnetic fields were merged into a single statistical sample, thereby obtaining the corresponding cumulative frequency distributions plotted in Figure 9. The *SCI* and *FCI* values for the soil sample are systematically greater than those for the biochar.

4 | Discussion

4.1 | Rill Erosion in Biochar-Amended Soils

The developed analysis stated that the addition of an initial biochar concentration of 5% can be considered a good soil conservation practice as it reduces soil erosion phenomena even if it produces an increase in *BC* in the eroded mixture. In other words, the increase in the initial *BC* (from 3% to 5%) has a positive effect on soil erosion and favours the preferential transport of the light biochar particles. These results do not agree with those obtained in previous experiments by Li et al. (2019, 2020), who demonstrated that lower biochar concentrations (1% and 3%) can inhibit soil erosion, while higher *BC* generally promotes erosive processes. The outcomes of this investigation are also different from those obtained by Gholamahmadi et al. (2023), who stated that biochar concentrations higher than 2.5% do not provoke a significant reduction in soil erosion. Instead, the results are coherent with those of the study by Zanutel and Bielders (2023), who highlighted that the increase in

TABLE 1 | Characteristic data of the investigated samples.

Sample	*BC* (%)	$m(T_A)$	$m(T_B)$	*m*(*SCI*)	*sd*(*SCI*)	*m*(*FCI*)	*sd*(*FCI*)
Soil	0	5.2	146.9	0.964	0.033	28.6	4.5
Mixture	1	7.6	183.2	1.012	0.076	27.2	6.5
Mixture	3	10.6	267.1	1.027	0.044	24.7	3.2
Mixture	5	12.7	312.5	1.054	0.017	24.6	5.1
Mixture	10	14.8	442.8	1.069	0.018	30.4	5.0
Mixture	30	18.3	485.1	1.016	0.025	26.3	6.7
Biochar	100	89.1	805.7	0.703	0.042	9.5	3.6

Note: $m(T_A)$ = mean value of T_A, $m(T_B)$ = mean value of T_B, *m*(*SCI*) = mean value of *SCI*, *m*(*FCI*) = mean value of *FCI*, *sd*(*SCI*) = standard deviation of *SCI*, *sd*(*FCI*) = standard deviation of *FCI*.

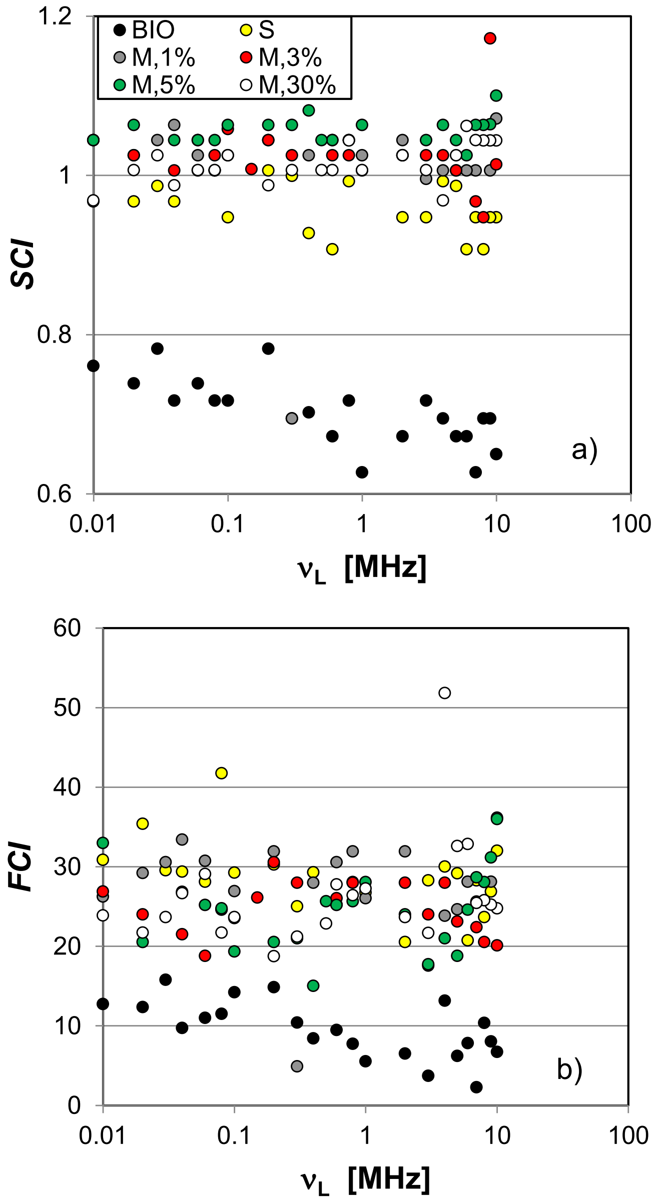

FIGURE 8 | Relationship between the applied proton Larmor frequency ν_L and structural connectivity index *SCI* (a) and functional connectivity index *FCI* (b) for all the investigated samples (biochar BIO, soil S, and mixture M, *x*, in which *x* is the biochar concentration).

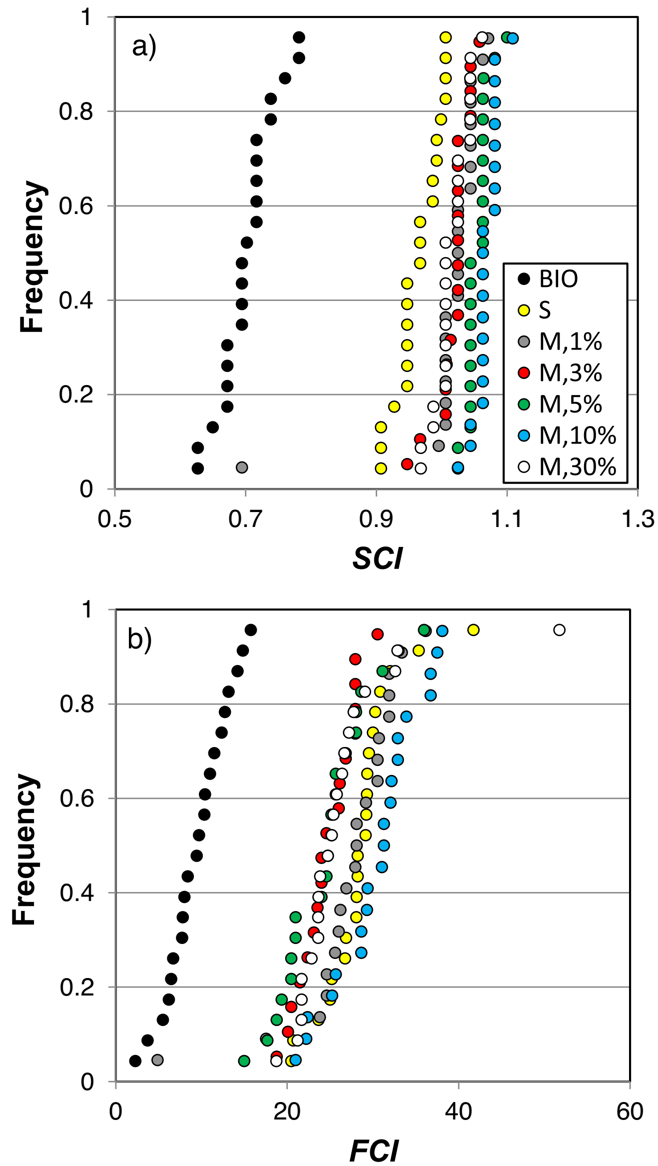

FIGURE 9 | Empirical frequency distributions of *SCI* (a) and *FCI* (b) for all the investigated samples (biochar BIO, soil S, and mixture *M*, *x*, in which *x* is the biochar concentration).

BC from 1% to 2% reduced interrill erosion for a sandy loam soil, while no effects were detected for a silt loam soil. It is worth noting that these literature results were obtained under simulated rainfall and not for rill flows. The experimental differences with the abovementioned studies (Li et al. 2019, 2020; Gholamahmadi et al. 2023) could justify the opposite trend found in this investigation. In any case, even if Zanutel and Bielders (2023) found the same trend as this study (i.e., the soil erosion decreases for increasing *BC* up to the investigated threshold) for other *BC* values, their results showed that soil erosion strictly depends on soil texture. In conclusion, the results of this study are roughly comparable with those reported in the cited literature.

The studies performed for rill flows by Li et al. (2021) and Parhizkar et al. (2023) did not investigate what happens when the biochar concentration increases from 3% to 5%. In detail, Li et al. (2021) found a decreased susceptibility to rill formation with the biochar addition up to $BC = 3\%$, while Parhizkar et al. (2023) found that biochar reduced rill erodibility, but they tested only a single *BC* value. Li et al. (2025), investigating the impact of *BC* on rill erodibility and critical shear stress, concluded that a 5.5% and 7% biochar addition increased K_r and reduced τ_c. In other words, *BC* values higher than the 5% threshold determine conditions in which soil resistance to rill erosion decreases, that is, biochar addition cannot be considered an effective soil conservation practice. In this sense, the result of the present study allows for demonstrating that the biochar concentration of 5% could represent the optimum for soil conservation strategies as it decreases soil loss, even if it produces a slightly higher biochar loss in the eroded volume. However, further studies should be performed to confirm the occurrence of this trend when the biochar concentration increases from 3% % to 5% and investigate what happens in field conditions for *BC* higher than 5%.

4.2 | Hydrological Connectivity of Biochar-Amended Soils

Figure 6 highlights that the shortest T_1 corresponds to the soil, while, on the contrary, the biochar is characterised by the longest T_1. Therefore, the mixtures M are characterised by longitudinal relaxation time values higher than those measured for the soil sample because of the increase in large-size pores in the M samples due to the presence of the biochar component. All $F(T_1)$ distributions are S-shaped and are always skewed towards shorter T_1, suggesting that, for each sample, the macro-pore component (largest T_1) is never dominant. The $F(T_1)$ distributions of the mixtures shift to the right with increasing values of the biochar component, and therefore the biochar addition increases the size of mesopores and micropores.

Figure 7 demonstrates that the mixtures with a biochar component of 3% and 5% are characterised by similar values of T_A and T_B with small differences compared to those detected for the series *M*, 30%. Thereby, increasing biochar beyond 5% only produces a small increase in T_A and T_B. This means that the biochar content of 5% can be considered a threshold value to obtain appreciable variations in the micro-pores and macro-pores compared to the original soil. In other words, 5% *BC* can be considered a threshold to change the soil structure and its effects on erosion processes. This result can be a precious tool to set, in agricultural field application, an optimum threshold of biochar concentration to add as soil amendment and soil conservation practice. In fact, according to the results of this investigation, the addition of biochar concentrations higher than 5% would be useless as it would not produce significant improvements in terms of soil structure. If future field investigations confirm that biochar concentrations higher than 5% would not further limit soil loss compared to $BC = 5\%$, the combination of these two results will allow for stating that adding biochar in concentrations higher than 5% would produce only an economic loss as it would not be justified by an increased effectiveness.

Figure 8a shows that the biochar addition improves the structural connectivity, and *SCI* reaches the maximum for $BC = 5\%$, while the lowest values are detected for $BC = 30\%$. Figure 8a also demonstrates that the structural connectivity index can be considered independent of the proton Larmor frequency. The representative mean value $m(SCI)$ and the standard deviation $sd(SCI)$ are listed in Table 1. Figure 8b shows how the functional connectivity index varies with ν_L, demonstrates that: (a) *FCI* is almost independent of the proton Larmor frequency and is characterised by the mean value $m(FCI)$ and the standard deviation $sd(FCI)$ listed in Table 1; (b) in the range $BC = 0\%–3\%$, the *FCI* decreases as *BC* increases. Figure 8 also points out that the NMR technique is able to discriminate the structural connectivity between soil and mixture.

Finally, Figure 9 highlights that, for increasing *BC* values up to 5%, *SCI* increases with increasing biochar (Figure 9a), while *FCI* decreases up to $BC = 3\%$ (Figure 9b). Therefore, biochar contents of 5% and 3% are discriminating values for *SCI* and *FCI*, respectively.

The developed analysis demonstrated that the FFC NMR technique is able to measure the two components, *SCI* and *FCI*, of the hydrological connectivity inside the soil and their differences due to the percentage of biochar.

5 | Conclusions

Even though there is an increasing interest in biochar as a soil amendment and a tool to improve soil structure and mitigate soil erosion, contrasting results on its significant usefulness as a soil conservation measure were reported in the literature. Furthermore, most of the existing experiments were carried out in interrill soil erosion conditions without paying particular attention to the concentration of biochar added to the original soils.

In this paper, the anti-erosive effectiveness of biochar was evaluated by rill measurements at the plot scale performed in soils amended with an initial biochar concentration in weight of 3% and 5%. The measurements demonstrated that the treatment with the higher initial biochar concentration (5%) decreases the overall erosive phenomenon and produces a higher biochar percentage in the eroded mixture. This result partially agrees with some of those available in the literature, while the differences as compared to other studies can be due to different experimental conditions (i.e., soil texture, flow type, etc.).

To investigate if the biochar concentration of 5% plays a significant role in the water movement inside the soil, which affects runoff and soil erosion processes, NMR relaxometry with the FFC layout was applied to measure the structural and functional connectivity of the soil and the biochar used in rill measurements, and mixtures with different biochar concentrations. These measurements demonstrated that the macro-pore component (longest T_1) is never dominant, and the biochar addition increases the size of mesopores and micropores. The biochar component improves the structural connectivity up to $BC = 5\%$, while the lowest values of the structural connectivity index are detected for $BC = 30\%$. The measurements also demonstrated that biochar preferentially improves the structural connectivity component, while it does not significantly vary the functional connectivity index for the mixtures as compared to that of soil.

In conclusion, a biochar concentration of 5% can mitigate the rill erosion phenomena, improve the soil structural connectivity, and not appreciably modify the functional connectivity.

Acknowledgements

All the authors contributed to outlining the investigation, analysing the data, discussing the results, and writing the manuscript. This research did not receive any specific grant from funding agencies in the public, commercial, or not-for-profit sectors. Open access publishing facilitated by Universita degli Studi di Palermo, as part of the Wiley - CRUI-CARE agreement.

Data Availability Statement

The data that support the findings of this study are available from the corresponding author upon reasonable request.

References

Abrol, V., M. Ben-Hur, F. G. A. Verheijen, et al. 2016. "Biochar Effects on Soil Water Infiltration and Erosion Under Seal Formation Conditions: Rainfall Simulation Experiment." *Journal of Soils and Sediments* 16: 2709–2719.

Atkinson, C. J., J. D. Fitzgerald, and N. A. Hipps. 2010. "Potential Mechanisms for Achieving Agricultural Benefits From Biochar Application to Temperate Soils: A Review." *Plant and Soil* 337: 1–18.

Baartman, J. E. M., R. Masselink, S. D. Keesstra, and A. J. A. M. Temme. 2013. "Linking Landscape Morphological Complexity and Sediment Connectivity." *Earth Surface Processes and Landforms* 38: 1457–1471. https://doi.org/10.1002/esp.3434.

Bagarello, V., and V. Ferro. 2010. "Analysis of Soil Loss Data From Plots of Different Length for the Sparacia Experimental Area, Sicily, Italy." *Biosystems Engineering* 105: 411–422.

Bagarello, V., G. V. Di Piazza, V. Ferro, and G. Giordano. 2008. "Predicting Unit Plot Soil Loss in Sicily, South Italy." *Hydrological Processes* 22: 586–595.

Bagarello, V., V. Ferro, G. Giordano, et al. 2011. "Effect of Plot Size on Measured Soil Loss for Two Italian Experimental Sites." *Biosystems Engineering* 108: 18–27.

Bagarello, V., C. Di Stefano, V. Ferro, and V. Pampalone. 2015. "Establishing a Soil Loss Threshold for Limiting Rilling." *Journal of Hydrologic Engineering* 20: C6014001.

Bagarello, V., V. Ferro, and D. C. Flanagan. 2018. "Predicting Plot Soil Loss by Empirical and Process-Oriented Approaches. A Review." *Journal of Agricultural Engineering (India)* XLIX, no. 710: 1–18.

Belisle, M. 2005. "Measuring Landscape Connectivity: The Challenge of Behavioural Landscape Ecology." *Ecology* 86: 1988–1995.

Blanco-Canqui, H. 2017. "Biochar and Soil Physical Properties." *Soil Science Society of America Journal* 81: 687–711.

Borgia, G. C., R. J. S. Brown, and P. Fantazzini. 1998. "Uniform-Penalty Inversion of Multiexponential Decay Data." *Journal of Magnetic Resonance* 132, no. 1: 65–77. https://doi.org/10.1006/jmre.1998.1387.

Borrelli, P., D. A. Robinson, L. R. Fleischer, et al. 2017. "An Assessment of the Global Impact of 21st Century Land Use Change on Soil Erosion." *Nature Communications* 8, no. 1: 2013.

Bracken, J., and J. Croke. 2007. "The Concept of Hydrological Connectivity and Its Contribution to Understanding Runoff-Dominated Geomorphic Systems." *Hydrological Processes* 21: 1749–1763. https://doi.org/10.1002/hyp.6313.

Bracken, L. J., J. Wainwright, G. A. Ali, et al. 2013. "Concepts of Hydrological Connectivity: Research Approaches, Pathways and Future Agendas." *Earth-Science Reviews* 119: 17–34. https://doi.org/10.1016/j.earscirev.2013.02.001.

Bruno, C., C. Di Stefano, and V. Ferro. 2008. "Field Investigation on Rilling in the Experimental Sparacia Area, South Italy." *Earth Surface Processes and Landforms* 33: 263–279.

Busscher, W. J., J. M. Novak, D. E. Evans, D. W. Watts, M. A. S. Niandou, and M. Ahmedna. 2010. "Influence of Pecan Biochar on Physical Properties of a Norfolk Loamy Sand." *Soil Science* 175: 10–14.

Carollo, F. G., C. Di Stefano, A. Nicosia, V. Palmeri, V. Pampalone, and V. Ferro. 2023. "A New Strategy to Assure Compliance With Soil Loss Tolerance at a Regional Scale." *Catena* 223: 106945. https://doi.org/10.1016/j.catena.2013.06.021.

Castellini, M., L. Giglio, M. Niedda, A. D. Palumbo, and D. Ventrella. 2015. "Impact of Biochar Addition on the Physical and Hydraulic Properties of a Clay Soil." *Soil and Tillage Research* 154: 1–13.

Conte, P. 2019. "Environmental Applications of Fast Field-Cycling NMR Relaxometry." In *Field-Cycling NMR Relaxometry: Instrumentation, Model Theories and Applications*, edited by R. Kimmich, 229–254. Royal Society of Chemistry.

Conte, P., and V. Ferro. 2018. "Measuring Hydrological Connectivity Inside a Soil by Low Field Nuclear Magnetic Resonance Relaxometry." *Hydrological Processes* 32: 93–101. https://doi.org/10.1002/hyp.11401.

Conte, P., and V. Ferro. 2020. "Standardizing the Use of Fast-Field Cycling NMR Relaxometry for Measuring Hydrological Connectivity Inside the Soil." *Magnetic Resonance in Chemistry* 58: 41–50. https://doi.org/10.1002/mrc.4907.

Conte, P., and V. Ferro. 2022. "Measuring Hydrological Connectivity Inside Soils With Different Texture by Fast Field Cycling Nuclear Magnetic Resonance Relaxometry." *Catena* 209: 105848. https://doi.org/10.1016/j.catena.2021.105848.

Conte, P., C. Di Stefano, V. Ferro, V. A. Laudicina, and E. Palazzolo. 2017. "Assessing Hydrological Connectivity Inside a Soil by Fast-Field-Cycling Nuclear Magnetic Resonance Relaxometry and Its Link to Sediment Delivery Processes." *Environment and Earth Science* 76: 526. https://doi.org/10.1007/s12665-017-6861-9.

De Pasquale, C., V. Marsala, A. E. Berns, et al. 2012. "Fast Field Cycling NMR Relaxometry Characterization of Biochars Obtained From an Industrial Thermochemical Process." *Journal of Soils and Sediments* 12: 1211–1221.

Di Stefano, C., and V. Ferro. 2016. "Establishing Soil Loss Tolerance: An Overview." *Journal of Agricultural Engineering* XLVII: 127–133. https://doi.org/10.4081/jae.2016.560.

Di Stefano, C., V. Ferro, V. Pampalone, and F. Sanzone. 2013. "Field Investigation of Rill and Ephemeral Gully Erosion in the Sparacia Experimental Area, South Italy." *Catena* 101: 226–234.

Di Stefano, C., V. Ferro, and V. Pampalone. 2015. "Modeling Rill Erosion at the Sparacia Experimental Area." *Journal of Hydrologic Engineering* 20: C5014001.

Di Stefano, C., V. Ferro, and V. Pampalone. 2016. "Measuring Field Rill Erodibility by a Simplified Method." *Land Degradation & Development* 27: 239–247.

Di Stefano, C., A. Nicosia, V. Pampalone, V. Palmeri, and V. Ferro. 2019. "New Technique for Measuring Water Depth in Rill Channels." *Catena* 181: 104090.

Di Stefano, C., A. Nicosia, V. Palmeri, V. Pampalone, and V. Ferro. 2022a. "Rill Flow Velocity and Resistance Law: A Review." *Earth-Science Reviews* 231: 104092.

Di Stefano, C., A. Nicosia, V. Palmeri, V. Pampalone, and V. Ferro. 2022b. "Rill Flow Resistance Law Under Sediment Transport." *Journal of Soils and Sediments* 22: 334–347.

Di Stefano, C., A. Nicosia, V. Pampalone, and V. Ferro. 2023. "Soil Loss Tolerance in the Context of the European Green Deal." *Heliyon* 9, no. 1: e12869.

Doan, T. T., T. Henry-des-Tureaux, C. Rumpel, J. L. Janeau, and P. Jouquet. 2015. "Impact of Compost, Vermicompost and Biochar on Soil Fertility, Maize Yield and Soil Erosion in Northern Vietnam: A Three Year Mesocosm Experiment." *Science of the Total Environment* 514: 147–154.

Gholamahmadi, B., S. Jeffery, O. Gonzales-Pelayo, et al. 2023. "Biochar Impacts on Runoff and Soil Erosion by Water: A Systematic Global Scale Meta-Analysis." *Science of the Total Environment* 871: 161860. https://doi.org/10.1016/j.scitotenv.2023.161860.

Govers, G., R. Giménez, and K. Van Oost. 2007. "Rill Erosion: Exploring the Relationship Between Experiments, Modeling and Field Observations." *Earth-Science Reviews* 8: 87–102.

Guerra, B., and K. Steenwerth. 2012. "Influence of Floor Management Technique on Grapevine Growth, Disease Pressure, and Juice and Wine Composition: A Review." *American Journal of Enology and Viticulture* 63, no. 2: 149–164.

Herath, H., M. Camps-Arbestain, and M. Hedley. 2013. "Effect of Biochar on Soil Physical Properties in Two Contrasting Soils: An Alfisol and an Andisol." *Geoderma* 209: 188–197.

Heri-Kazi, A. B., and C. L. Bielders. 2021. "Cropland Characteristics and Extent of Soil Loss by Rill and Gully Erosion in Smallholder Farms in the KIVU Highlands, DR Congo." *Geoderma Regional* 26: e00404.

Hseu, Z. Y., S. H. Jien, W. H. Chien, and R. C. Liou. 2014. "Impacts of Biochar on Physical Properties and Erosion Potential of a Mudstone Slopeland Soil." *Scientific World Journal* 2014: 602197.

Huang, Y., X. Chen, B. Luo, L. Ding, and C. Gong. 2015. "An Experimental Study of Rill Sediment Delivery in Purple Soil, Using the Volume-Replacement Method." *PeerJ* 3: e1220.

Jien, S. H., and C. S. Wang. 2013. "Effects of Biochar on Soil Properties and Erosion Potential in a Highly Weathered Soil." *Catena* 110: 225–233.

Joseph, S. D., M. Camps-Arbestain, Y. Lin, et al. 2010. "An Investigation Into the Reactions of Biochar in Soil." *Soil Research* 48, no. 7: 501–515.

Keesstra, S. S., V. Bagarello, V. Ferro, D. Finger, and A. J. Parsons. 2020. "Connectivity in Hydrology and Sediment Dynamics." *Land Degradation and Development* 31: 2525–2528. https://doi.org/10.1002/ldr.3401.

Laudicina, V. A., C. De Pasquale, P. Conte, L. Badalucco, G. Alonzo, and E. Palazzolo. 2012. "Effects of Afforestation With Four Unmixed Plant Species on the Soil–Water Interactions in a Semiarid Mediterranean Region (Sicily, Italy)." *Journal of Soils and Sediments* 12: 1222–1230.

Lee, S. S., H. S. Shah, Y. M. Awad, S. Kumar, and Y. S. Ok. 2015. "Synergy Effects of Biochar and Polyacrylamide on Plants Growth and Soil Erosion Control." *Environment and Earth Science* 74: 2463–2473.

Lee, C. H., C. C. Wang, H. H. Lin, et al. 2018. "In-Situ Biochar Application Conserves Nutrients While Simultaneously Mitigating Runoff and Erosion of an Fe-Oxide-Enriched Tropical Soil." *Science of the Total Environment* 619–620: 665–671.

Li, Q. X., Z. W. Jin, X. M. Chen, Y. Jing, Q. R. Huang, and J. B. Zhang. 2017. "Effects of Biochar on Aggregate Characteristics of Upland Red Soil in Subtropical China." *Environment and Earth Science* 76: 372.

Li, Y. Y., F. B. Zhang, M. Y. Yang, J. Q. Zhang, and Y. G. Xie. 2019. "Impacts of Biochar Application Rates and Particle Sizes on Runoff and Soil Loss in Small Cultivated Loess Plots Under Simulated Rainfall." *Science of the Total Environment* 649: 1403–1413.

Li, Y., G. Feng, H. Tewoldec, M. Yang, and F. Zhang. 2020. "Soil, Biochar, and Nitrogen Loss to Runoff From Loess Soil Amended With Biochar Under Simulated Rainfall." *Journal of Hydrology* 591: 125318.

Li, T., P. Yu, D. Liu, et al. 2021. "Effects of Biochar on Sediment Transport and Rill Erosion After Two Consecutive Years of Seasonal Freezing and Thawing." *Sustainability* 13: 6984.

Li, Y., Y. yuan, J. Zhao, et al. 2025. "Biochar Addition Enhances Silt Loam Resistance to Rill Flow: A Study Based on Three Years of Field Monitoring Data on China's Loess Plateau." *Soil & Tillage Research* 245: 106320.

López-Vicente, M., E. Nadal-Romero, and E. L. H. Cammeraat. 2017. "Hydrological Connectivity Does Change Over 70 Years of Abandonment and Afforestation in the Spanish Pyrenees." *Land Degradation and Development* 28: 1298–1310. https://doi.org/10.1002/ldr.2531.

Lu, H., I. P. Prosser, C. J. Moran, J. C. Gallant, G. Priestley, and J. G. Stevenson. 2003. "Predicting Sheetwash and Rill Erosion Over the Australian Continent." *Soil Research* 41, no. 6: 1037–1062.

Marchamalo, M., J. M. Hooke, and P. J. Sandercock. 2016. "Flow and Sediment Connectivity in Semi-Arid Landscapes in SE Spain: Patterns and Controls." *Land Degradation and Development* 27: 1032–1044. https://doi.org/10.1002/ldr.2352.

Mutchler, C. K., and R. A. Young. 1975. "Soil Detachment by Raindrops." In *Present and Prospective Technology for Predicting Sediment Yields and Sources*, 113–117. USDA Sedimentation Laboratory: ARS-S-40.

Nicosia, A., V. Pampalone, and V. Ferro. 2021. "Effects of Biochar Addition on Rill Flow Resistance." *Water* 13, no. 21: 3036. https://doi.org/10.3390/w13213036.

Novara, A., A. Cerda, E. Barone, and L. Gristina. 2021. "Cover Crop Management and Water Conservation in Vineyard and Olive Orchards." *Soil and Tillage Research* 208: 104896.

Pagliai, M., and N. Vignozzi. 2002. "The Soil Pore System as an Indicator of Soil Quality." In *Sustainable Land Management-Environmental Protection. A Soil Physical Approach*, edited by M. Pagliai and R. Jones, 71–82. IUSS, Advances in GeoEcology.

Parhizkar, M., M. Shabanpour, M. E. Lucas-Borja, et al. 2021. "Effects of Length and Application Rate of Rice Straw Mulch on Surface Runoff and Soil Loss Under Laboratory Simulated Rainfall." *International Journal of Sediment Research* 36, no. 4: 468–478.

Parhizkar, M., M. Shabanpour, M. E. Lucas-Borja, and D. A. Zema. 2023. "Effects of Rice Husk Biochar on Rill Detachment Capacity in Deforested Hillslopes." *Ecological Engineering* 191: 106964.

Peng, W., Z. Zhang, and K. Zhang. 2015. "Hydrodynamic Characteristics of Rill Flow on Steep Slopes." *Hydrological Processes* 29: 3677–3686.

Pimentel, D. 2006. "Soil Erosion: A Food and Environmental Threat." *Environment, Development and Sustainability* 8: 119–137.

Pohlmeier, A., S. Haber-Pohlmeier, and S. Stapf. 2009. "A Fast Field Cycling Nuclear Magnetic Resonance Relaxometry Study of Natural Soils." *Vadose Zone Journal* 8: 735–742. https://doi.org/10.2136/vzj2008.0030.

Polyakov, V. O., and M. A. Nearing. 2003. "Sediment Transport in Rill Flow Under Deposition and Detachment Conditions." *Catena* 51, no. 1: 33–43.

Pringle, C. 2003. "What Is Hydrologic Connectivity and Why Is It Ecologically Important?" *Hydrological Processes* 17: 2685–2689. https://doi.org/10.1002/hyp.5145.

Reaney, S. M., L. J. Bracken, and M. J. Kirkby. 2014. "The Importance of Surface Controls on Overland Flow Connectivity in Semi-Arid Environments: Results From a Numerical Experimental Approach." *Hydrological Processes* 28: 2116–2128. https://doi.org/10.1002/hyp.9769.

Sadeghi, S. H. R., Z. Hazbavi, and M. K. Harchegani. 2016. "Controllability of Runoff and Soil Loss From Small Plots Treated by Vinasse-Produced Biochar." *Science of the Total Environment* 541: 483–490.

Schmidt, H. P., C. Kammann, C. Niggli, M. W. Evangelou, K. A. Mackie, and S. Abiven. 2014. "Biochar and Biochar-Compost as Soil Amendments to a Vineyard Soil: Influences on Plant Growth, Nutrient Uptake, Plant Health and Grape Quality." *Agriculture, Ecosystems & Environment* 191: 117–123.

Smetanová, A., M. Dotterweich, D. Diehl, U. Ulrich, and N. Fohrer. 2013. "Influence of Biochar and Terra Preta Substrates on Wettability and Erodibility of Soils." *Zeitschrift für Geomorphologie* 57: 111–134.

Sohi, S. P., E. Krull, E. Lopezcapel, and R. Bol. 2010. "A Review of Biochar and Its Use and Function in Soil." *Advances in Agronomy* 105: 47–82.

Turnbull, L., J. Wainwright, and R. E. Brazier. 2008. "A Conceptual Framework for Understanding Semi-Arid Land Degradation: Ecohydrological Interactions Across Multiple-Space and Time Scales." *Ecohydrology* 1: 23–34. https://doi.org/10.1002/eco.4.

Uezu, A., J. P. Metzger, and J. M. E. Vielliard. 2005. "Effects of Structural and Functional Connectivity and Patch Size on the Abundance of Seven Atlantic Forest Bird Species." *Biological Conservation* 123: 507–519.

Waddington, D. V. 1992. "Soils, Soil Mixtures, and Soil Amendments." *Turfgrass* 32: 331–383.

Wainwright, J., L. Turnbull, T. G. Ibrahim, I. Lexartza-Artza, S. F. Thornton, and R. E. Brazier. 2011. "Linking Environmental régimes, Space and Time: Interpretations of Structural and Functional Connectivity." *Geomorphology* 126: 387–404. https://doi.org/10.1016/j.geomorph.2010.07.027.

Wang, J., and S. Wang. 2019. "Preparation, Modification and Environmental Application of Biochar: A Review." *Journal of Cleaner Production* 227: 1002–1022.

Wani, I., S. R. Narde, X. Huang, N. Remya, V. Kushvaha, and A. Garg. 2021. "Reviewing Role of Biochar in Controlling Soil Erosion and Considering Future Aspect of Production Using Microwave Pyrolysis Process for the Same." *Biomass Conversion and Biorefinery* 13, no. 13: 11543–11569. https://doi.org/10.1007/s13399-021-02060-1.

Wirtz, S., T. Iserloh, G. Rock, et al. 2012. "Soil Erosion on Abandoned Land in Andalusia: A Comparison of Interrill-and Rill Erosion Rates." *International Scholarly Research Notices* 2012, no. 1: 730870.

Zanutel, M., and C. L. Bielders. 2023. "Contrasted Effects of Biochar Application on Interrill Erosion Depending on Age, Application Rate and Soil Type." *Geoderma Regional* 34: e00706. https://doi.org/10.1016/j.geodrs.2023.e00706.

Zhang, P., H. Tang, W. Yao, N. Zhang, and L. V. Xizhi. 2016. "Experimental Investigation of Morphological Characteristics of Rill Evolution on Loess Slope." *Catena* 137: 536–544.

Zhang, F., C. Huang, M. Yang, J. Zhang, and W. Shi. 2019. "Rainfall Simulation Experiments Indicate That Biochar Addition Enhances Erosion of Loess-Derived Soils." *Land Degradation & Development* 30, no. 30: 2272–2286.